SCIENCE CHINA
Technological Sciences

March 2013 Vol.56 No.3: 666–676
doi: 10.1007/s11431-012-5091-3

Effect of driving conditions and suspension parameters on dynamic load-sharing of longitudinal-connected air suspensions

CHEN YiKai[1,2*], HE Jie[3], KING Mark[4], CHEN WuWei[5] & ZHANG WeiHua[1]

[1] *School of Transportation Engineering, Hefei University of Technology, Hefei 230009, China;*
[2] *Traffic Management Research Institute of the Ministry of Public Security, Wuxi 214151, China;*
[3] *School of Transportation, Southeast University, Nanjing 210096, China;*
[4] *Centre for Accident Research and Road Safety-Queensland, Queensland University of Technology, Kelvin Grove 4059, Australia;*
[5] *School of Mechanical and Automotive Engineering, Hefei University of Technology, Hefei 230009, China*

Received August 16, 2012; accepted November 5, 2012; published online December 18, 2012

The objective of this research was to investigate the effects of driving conditions and suspension parameters on dynamic load-sharing of longitudinal-connected air suspensions of a tri-axle semi-trailer. A novel nonlinear model of a multi-axle semi-trailer with longitudinal-connected air suspension was formulated based on fluid mechanics and thermodynamics and was validated through test results. The effects of driving conditions and suspension parameters on dynamic load-sharing and road-friendliness of the semi-trailer were analyzed. Simulation results indicate that the road-friendliness metric–DLC (dynamic load coefficient) is not always in accordance with the load-sharing metric–DLSC (dynamic load-sharing coefficient). The effect of employing larger air lines and connectors on the DLSC optimization ratio gives varying results as road roughness increases and as driving speed increases. When the vehicle load reduces, or the static pressure increases, the DLSC optimization ratio declines monotonically. The results also indicate that if the air line diameter is always assumed to be larger than the connector diameter, the influence of air line diameter on load-sharing is more significant than that of the connector.

driving condition, dynamic load-sharing, longitudinal-connected air suspension, heavy truck

Citation: Chen Y K, He J, King M, et al. Effect of driving conditions and suspension parameters on dynamic load-sharing of longitudinal-connected air suspensions. Sci China Tech Sci, 2013, 56: 666–676, doi: 10.1007/s11431-012-5091-3

1 Introduction

Extensive studies of "road-friendly" heavy vehicles have been performed during the last few decades to reduce road damage and increase the rated load of vehicles. However, the load-sharing ability of multi-axle heavy vehicles, which has a strong correlation with road-friendliness, has been far from being adequately investigated. Load-sharing is defined as the equalization of the axle group load across all wheels/axles [1]. When a multi-axle heavy vehicle with leaf suspensions travels on a rough road or hits a bump/ pothole, such as a bridge-head, or speed control humps, unequally distributed loads among the axles of an axle group tend to appear due to the ineffectiveness of the load-sharing mechanism (centrally pivoted walking beam, trunnion shaft, etc.) and the high stiffness of leaf springs [2]. This phenomenon causes overloading of a single axle of the axle group, which has at least two disadvantages: (a) It increases the possibility of a tire bursting as well as reducing the maneuverability and stability of the vehicle; (b) it accelerates the rutting and fatigue that contributes to pavement damage [3]. As a consequence, the improvement of load-sharing within axle groups has attracted much attention among both vehicle

*Corresponding author (email: leochen079307@hotmail.com)

manufacturers and road management departments.

Load-sharing performances of axle groups are specified in regulations for road-friendly vehicles in many countries. The DIVINE (Dynamic Interaction between Vehicle and Infrastructure Experiment) project undertaken by OECD (Organization for Economic Cooperation and Development) suggests that to qualify as a road-friendly tandem suspension, the average load variation per unit of relative vertical suspension displacement must be less than 0.3 kN/mm [4]. The Australian specification for road-friendly suspensions nominates that road-friendly suspensions must have static load-sharing, i.e., load-sharing when the vehicle is stationary, to a defined value, between axles in an axle group or tires in an axle group. However, the formal methodology to determine the static load-sharing value on a heavy vehicle is not defined [5]. In Europe, an air suspension needs to have fully-functioning hydraulic shock absorbers to pass a static road-friendliness test [6], and heavy vehicles with road-friendly suspensions are allowed higher static axle loads. A common problem for these regulations is that only the static load-sharing of vehicles is specified, there is no requirement for suspensions to retain their dynamic load-sharing performance, i.e., load-sharing when the vehicle is driving.

Many other load-sharing metrics have also been proposed by researchers. LSC (load-sharing coefficient) [7] and DLSC (dynamic load-sharing coefficient) [8] have been used to evaluate static and dynamic load-sharing, respectively. Note that perfect load equalization would give a LSC of 1.0 [9]; LSC values for steel suspensions were documented in the range 0.791 to 0.957 [7]. Air suspensions with conventional-size longitudinal air lines were placed in the middle of this range with LSCs of 0.904 to 0.925 [10]. More recent studies commissioned by the National Road Transport Commission of Australia found that installation of larger air lines on multi-axle air suspensions increased longitudinal air flow between air springs on adjacent axles [11, 12]. Follow-up tests funded by the Queensland Department of Main Roads discovered that an improvement in DLSC of 4%–30% for a tri-axle coach and 37%–77% for a tri-axle semi-trailer were obtained by alternating the conventional-size longitudinal air connection (three 6.5 mm inside diameter connectors connecting 6.5 mm inside diameter air lines) with a larger air connection (three 20 mm inside diameter connectors connecting 50 mm inside diameter air lines) [13, 14]. However, due to the limitations of laboratory equipment, only vehicle speed and a limited number of air connections were considered in most tests, such that the effect of some other factors, such as the static absolute air pressure of the air spring, static height of the air spring, road class, and vehicle load, on load-sharing have not yet been reported before.

Limitations of laboratory and on-road tests can be addressed by developing realistic models of longitudinal-connected air suspensions. Potter et al. developed a simplified tandem bogie model, and by changing the damping coefficient and torsional stiffness of the leveling beam of the model [2], it can represent load-leveling steel suspensions, independent steel suspensions, longitudinal-connected air suspensions, and independent air suspensions, respectively. Davis proposed a model of a tri-axle semi-trailer with longitudinal-connected air suspensions [13], and used a variable "load-sharing fraction" to represent the load-sharing ability of the suspension. However, the physical meaning of the variable was unclear. A more realistic model of a similar tri-axle semi-trailer was developed by Roebuck et al. based on aerodynamics and thermodynamics [15]. In the model, the volumetric flow rate (m^3/s) between two air springs was assumed to be simply proportional to the difference in air pressure with a constant coefficient C_{flow} (m^3/kPa s); in addition, the volumes and effective areas of the air springs were simplified as constants while the vehicle was travelling.

Unfortunately, these simplifications of nonlinearities reduced the precision of the proposed models. A more realistic model of longitudinal-connected multi-axle air suspensions is urgently needed for precise analysis and optimization of load-sharing in multi-axle semi-trailers.

The rest of this paper is organized in the following order. In Section 2, a novel nonlinear model of longitudinal-connected tri-axle air suspensions is derived based on fluid mechanics and thermodynamics. The accuracy of the model is validated and load-sharing criteria are chosen in Section 3. Based on the model, the effects of driving conditions (road class, vehicle speed and vehicle load) and air suspension parameters (static height and static absolute air pressure of air spring, inside diameters of air line and connector) on dynamic load-sharing are analyzed in Section 4 and Section 5, respectively. Finally, Section 6 presents a summary of the results and draws conclusions.

2 Integrated model of vehicle and road excitation

2.1 Mathematic model of the tri-axle semi-trailer

A basic half model representing a typical tri-axle semi-trailer with longitudinal-connected air suspensions in most western countries was employed, as shown in Figure 1. This model includes five degrees of freedom (DOF), which are vertical displacement of sprung mass and three unsprung masses, z, x_1, x_2, x_3, as well as the pitch angle of the sprung mass ϕ.

The equations of motion of the semi-trailer are given by

$$m_{t1}\ddot{x}_1 = (q_1 - x_1)k_{t1} + c_1(\dot{z} - \dot{x}_1 - \dot{\phi}l) - (P_{s1} - P_0)A_{s1} + \frac{1}{3}mg, \quad (1)$$

$$m_{t2}\ddot{x}_2 = (q_2 - x_2)k_{t2} + c_2(\dot{z} - \dot{x}_2) - (P_{s2} - P_0)A_{s2} + \frac{1}{3}mg, \quad (2)$$

$$m_{t3}\ddot{x}_3 = (q_3 - x_3)k_{t3} + c_3(\dot{z} - \dot{x}_3 + \dot{\phi}l) - (P_{s3} - P_0)A_{s3} + \frac{1}{3}mg, \quad (3)$$

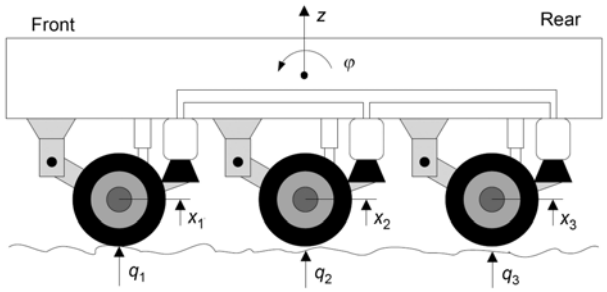

Figure 1 Schematic of the tri-axle semi-trailer with longitudinal-connected air suspensions.

$$J\ddot{\phi} = \left[(P_{s3}-P_0)A_{s3} - c_3(\dot{z}-\dot{x}_3+\dot{\phi}l) - \frac{1}{3}mg\right]l - \left[(P_{s1}-P_0)A_{s1} - c_1(\dot{z}-\dot{x}_1-\dot{\phi}l) - \frac{1}{3}mg\right]l, \quad (4)$$

$$m\ddot{z} = (P_{s1}-P_0)A_{s1} + (P_{s2}-P_0)A_{s2} + (P_{s3}-P_0)A_{s3} - c_1(\dot{z}-\dot{x}_1-\dot{\phi}l) - c_2(\dot{z}-\dot{x}_2) - c_3(\dot{z}-\dot{x}_1-\dot{\phi}l) - mg, \quad (5)$$

where m_{t1}, m_{t2}, m_{t3} and q_1, q_2, q_3 are the unsprung masses and road excitations of the three axles, respectively. m is the sprung mass of the semi-trailer. J is the moment of inertia of the gross sprung mass around the lateral axis. P_{s1}, P_{s2}, P_{s3} and A_{s1}, A_{s2}, A_{s3} are the dynamic absolute air pressures and dynamic effective areas of the three air springs, respectively. P_0 is atmospheric pressure. l is the wheelbase, c_1, c_2, c_3 are the damping coefficients of three dampers, and k_{t1}, k_{t2}, k_{t3} are the stiffness of the three tires.

2.2 Road roughness excitation

Many methodologies have been proposed to model road surface profile [16–18]. One method is to describe the profile as a realization of a random process that is represented by its PSD (power spectral density). A concise spectral model is used in this study as [19]

$$G_q(n) = G_q(n_0)\left(\frac{n}{n_0}\right)^{-2} \quad (n_1 < n < n_2), \quad (6)$$

where $G_q(n)$ is the PSD function (m^3/cycle) for the road surface elevation; n is the spatial frequency (cycle/m); n_0 is the reference spatial frequency, n_0=0.1 cycle/m; $G_q(n_0)$ is roughness coefficient (m^3/cycle), whose value is chosen depending on the road condition. Classification of road roughness is based on the index of the International Organization for Standardization [20]. The ISO has proposed a road roughness classification from Class "A" (very good) to Class "H" (very poor) according to different values of $G_q(n_0)$. n_1 and n_2 are lower and upper spatial cutoff frequencies when $G_q(n)$ reaches 1 m^3/cycle and 10^{-5} m^3/cycle, respectively [20].

When travelling along the road surface at a constant vehicle speed u, the temporal frequencies f and n are related as f=un. Therefore, the relationship between spatial PSD and temporal PSD becomes

$$G_q(f) = \frac{1}{u}G_q(n) = \frac{1}{u}G_q(n_0)\left(\frac{n}{n_0}\right)^{-2} = G_q(n_0)n_0^2\frac{u}{f^2}. \quad (7)$$

As the angular frequency ω is related to f as ω=2πf, eq. (7) is rewritten as

$$G_q(\omega) = 4\pi^2 G_q(n_0)n_0^2\frac{u}{\omega^2}. \quad (8)$$

Eq. (8) is transformed to the following equation when inserting a lower cutoff angular frequency ω_1 [21]:

$$G_q(\omega) = 4\pi^2 G_q(n_0)n_0^2\frac{u}{\omega^2+\omega_1^2}, \quad (9)$$

where ω_1=2πn_1u. Standard road roughness is a response of a first order linear to a white noise $w(t)$ [22], therefore

$$G_q(\omega) = |H(\omega)|^2 S_\omega, \quad (10)$$

where S_ω is the PSD of the white noise, S_ω =1. Substituting eq. (10) into eq. (9) yields

$$H(\omega) = \frac{2\pi n_0\sqrt{G_q(n_0)u}}{\omega_1 + j\omega}. \quad (11)$$

Then the road roughness $q(t)$ is given by

$$\dot{q}(t) = -2\pi n_1 u q(t) + 2\pi n_0\sqrt{G_q(n_0)u}\,w(t). \quad (12)$$

The upper cutoff frequency n_2 was modeled by setting the sampling frequency of $w(t)$ based on Nyquist sampling theory, i.e., the sampling frequency should be at least $2n_2u$ Hz. A time delay of l/v for road excitation is applied between adjacent axles.

2.3 Detailed model of longitudinal-connected tri-axle air suspensions

To solve the equations in Section 2.1, a detailed model of longitudinal-connected tri-axle air suspensions is needed to express P_{s1}, P_{s2} and P_{s3} as functions of the 5 variables (5 DOF).

It is assumed that all the air springs are stroked fast enough such that all of the heat of the operation is conserved when the vehicle is travelling, i.e., an adiabatic process occurs. Thus, the formula for calculating the dynamic absolute air pressure inside the front air spring P_{s1} is [23]

$$P_{s1}\left(\frac{V_{s1}}{m_{s1}}\right)^k = P_{s10}\left(\frac{V_{s10}}{m_{s10}}\right)^k = \text{constant}, \quad (13)$$

where V_{s1}, V_{s10} are the dynamic volume, and static volume of the front air spring; m_{s1}, m_{s10} are the dynamic air mass, and static air mass inside the front air spring; and P_{s10} is the static absolute air pressure inside the front air spring. The value of the above exponent k varies with the gas used and is a function of the specific heat of the gas. Air suspension operation is characterized by neither an isothermal nor an adiabatic process, but it is instead polytropic. In normal use, however, the process is much closer to adiabatic than isothermal. Accordingly the value of k is set to 1.4.

P_{s1} is obtained from eq. (13) as follows:

$$P_{s1}=\left(\frac{V_{s10}m_{s1}}{V_{s1}m_{s10}}\right)^{1.4}P_{s10}, \tag{14}$$

where V_{s1} is a function of the dynamic height of the front air spring, and is given by

$$V_{s1}=(z-x_1-\phi l)A_{s1}+V_{s10}, \tag{15}$$

where A_{s1} can also be approximated as a function of dynamic height based on experimental data. m_{s1} depends on the air flow rate inside the front connector G_1(kg/s) and is given by

$$m_{s1}=m_{10}+\int_0^t G_1\mathrm{d}t. \tag{16}$$

Since only small variations of temperature, air pressure and air spring volume exist when the semi-trailer is travelling, the air flow inside the front connector is considered to be an incompressible steady flow, which satisfies the following formula, according to Bernoulli's equation [24]:

$$\frac{P_{s1}}{\rho}+\frac{1}{2}v_{s1}^2=\frac{P_{f1}}{\rho}+\frac{1}{2}v_{f1}^2, \tag{17}$$

where P_{f1} is the dynamic absolute air pressure inside the front connector; v_{s1}, v_{f1} are the air flow speeds (m/s) inside the front air spring and the front connector, respectively; and the air inside all the air springs, connectors and the air line is assumed to have a same constant density ρ, when the semi-trailer is travelling; A_{f1} is the effective area of the front connector, which is equal to the actual area multiplied by a contraction coefficient 0.7 [25].

Note that A_{s1} is related to A_{f1} because $A_{s1}v_{s1}$=$A_{f1}v_{f1}$; inserting v_{s1}=$A_{f1}v_{f1}$/A_{s1} into eq. (17) yields

$$v_{f1}=\sqrt{\frac{2}{\rho}\left|P_{s1}-P_{f1}\right|\Big/\left[1-\left(\frac{A_{f1}^2}{A_{s1}^2}\right)\right]}. \tag{18}$$

v_{f1} is modified with a coefficient c_d (0.8) to reflect the friction of the connector. Therefore, the actual air flow speed inside the front connector v'_{f1} and G_1 are given by

$$v'_{f1}=c_d\sqrt{\frac{2}{\rho}\left|P_{s1}-P_{f1}\right|\Big/\left[1-\left(\frac{A_{f1}^2}{A_{s1}^2}\right)\right]}, \tag{19}$$

$$G_1=\mathrm{sgn}(P_{f1}-P_{s1})c_dA_{f1}\sqrt{2\rho\left|P_{s1}-P_{f1}\right|\Big/\left[1-\left(\frac{A_{f1}^2}{A_{s1}^2}\right)\right]}. \tag{20}$$

Substituting eqs. (15), (16) and (20) into eq. (14) yields

$$P_{s1}=P_{s10}\left(\frac{V_{s10}\left[m_{10}+\int_0^t\mathrm{sgn}(P_{f1}-P_{s1})c_dA_{f1}\sqrt{2\rho\left|P_{s1}-P_{f1}\right|\Big/\left(1-\left(\frac{A_{f1}^2}{A_{s1}^2}\right)\right)}\mathrm{d}t\right]}{\left[(z-x_1-\phi l)A_{s1}+V_{s10}\right]m_{s10}}\right)^{1.4}. \tag{21}$$

The dynamic absolute air pressures inside the three connectors and the longitudinal air line are assumed to have the same value P_{f1} during travel. Thus, similar expressions for the air flow rates inside the middle and rear connectors (G_2 and G_3), as well as the dynamic absolute air pressures inside the middle and rear air springs (P_{s2} and P_{s3}) are derived as follows:

$$G_2=\mathrm{sgn}(P_{f1}-P_{s2})c_dA_{f2}\sqrt{2\rho\left|P_{s2}-P_{f1}\right|\Big/\left[1-\left(\frac{A_{f2}^2}{A_{s2}^2}\right)\right]}, \tag{22}$$

$$G_3=\mathrm{sgn}(P_{f1}-P_{s3})c_dA_{f3}\sqrt{2\rho\left|P_{s3}-P_{f1}\right|\Big/\left[1-\left(\frac{A_{f3}^2}{A_{s3}^2}\right)\right]}, \tag{23}$$

$$P_{s2}=P_{s20}\left(\frac{V_{s20}\left[m_{20}+\int_0^t\mathrm{sgn}(P_{f1}-P_{s2})c_dA_{f2}\sqrt{2\rho\left|P_{s2}-P_{f1}\right|\Big/\left(1-\left(\frac{A_{f2}^2}{A_{s2}^2}\right)\right)}\mathrm{d}t\right]}{\left[(z-x_2)A_{s2}+V_{s20}\right]m_{s20}}\right)^{1.4}, \tag{24}$$

$$P_{s3}=P_{s30}\left(\frac{V_{s30}\left[m_{30}+\int_0^t\mathrm{sgn}(P_{f1}-P_{s3})c_dA_{f3}\sqrt{2\rho\left|P_{s3}-P_{f1}\right|\Big/\left(1-\left(\frac{A_{f3}^2}{A_{s3}^2}\right)\right)}\mathrm{d}t\right]}{\left[(z-x_3+\phi l)A_{s3}+V_{s30}\right]m_{s30}}\right)^{1.4}, \tag{25}$$

where P_{s20}, V_{s20}, m_{s20} are the static absolute air pressure, static volume and static air mass of the middle air spring, P_{s30}, V_{s30}, m_{s30} are the corresponding parameters for the rear air spring; and A_{f2}, A_{f3} are the areas of the middle and rear connectors, respectively. The three air springs have the same static absolute air pressure, static volume and static air mass, and the three connectors have the same inside diameter.

The air line is made of steel, so the volume of air line is constant. Based on eq. (14), the dynamic absolute air pressure inside the air line P_{f1} is expressed as a function of the static air mass of the air line m_{l0}, the static absolute air pressure inside the air line P_{s10}, and the gross air flow rate inside the air line G_1:

$$P_{f1}=\left(\frac{m_{l0}+\int_0^t G_1 \mathrm{d}t}{m_{l0}}\right)^{1.4} P_{s10}, \tag{26}$$

$$G_1=-G_1-G_2-G_3. \tag{27}$$

Substituting eqs. (20), (22), (23) and (27) into eq. (26) yields:

$$P_{f1}=m_{l0}^{-1.4}P_{sl0}\left(m_{l0}+\int_0^t\left\{-\mathrm{sgn}(P_{f1}-P_{s1})c_d A_{f1}\sqrt{2\rho\left|P_{s1}-P_{f1}\right|\Big/\left[1-\left(\frac{A_{f1}^2}{A_{s1}^2}\right)\right]}-\mathrm{sgn}(P_{f1}-P_{s2})c_d A_{f2}\right.\right.$$
$$\left.\left.\sqrt{2\rho\left|P_{s2}-P_{f1}\right|\Big/\left[1-\left(\frac{A_{f2}^2}{A_{s2}^2}\right)\right]}-\mathrm{sgn}(P_{f1}-P_{s3})c_d A_{f3}\sqrt{2\rho\left|P_{s3}-P_{f1}\right|\Big/\left[1-\left(\frac{A_{f3}^2}{A_{s3}^2}\right)\right]}\right\}\mathrm{d}t\right)^{1.4}. \tag{28}$$

Based on the equations in Sections 2.1, 2.2 and eqs. (21), (24), (25) and (28), an integrated model of road excitation and a fully-loaded tri-axle semi-trailer with longitudinal-connected air springs was developed with Matlab/Simulink. Parts of the key parameters are tabulated in Table 1. The expression of the effective area of each air spring as a function of the dynamic height of corresponding air spring will be obtained based on test results in Section 3.2.

Table 1 Parameters of the tri-axle semi-trailer model

Parameter	Value	Dimension	Description
A_{s10}	0.0783	m^2	static effective area of each air spring
V_{s10}	0.0125	m^3	static volume of each air spring
h_{s0}	0.16	m	static height of each air spring
d_f	0.0065	m	inside diameter of each connector
d_s	0.0065	m	inside diameter of the longitudinal air line
P_{s10}	464288	Pa	static absolute air pressure inside each air spring, each connector and the air line
P_0	101325	Pa	atmosphere pressure
m	8700	kg	gross sprung mass of the semi-trailer
m_{t1}	336	kg	unsprung mass of each air spring
J	5684	kg m^2	moment of inertia of the gross sprung mass around the lateral axis
k_{t1}	1960000	N/m	stiffness of dual tires on each hub
ρ	6.5417	kg/m^3	density of air inside air springs, air connectors and the air line
$c_{rebound}$	288600	N s/m	damping coefficient of each damper when dynamic height of respective suspension is increasing
c_{bump}	184500	N s/m	damping coefficient of each damper when dynamic height of respective suspension is decreasing

3 Load-sharing criteria and model validation

3.1 Load-sharing criteria

Criteria need to be chosen to evaluate the load-sharing of the semi-trailer. A metric often used to characterize the magnitude of dynamic forces of a wheel in an axle group is the DLC (dynamic load coefficient) [7], defined as

$$DLC(i)=\frac{\sigma_i}{F_{\mathrm{mean}}(i)}, \tag{29}$$

where σ_i denotes the standard deviation of wheel-force i, and $F_{\mathrm{mean}}(i)$ denotes the mean wheel-force of wheel i. Although DLC is usually referred to as a road-friendliness criterion and has been criticized for its mutual exclusivity with another load-sharing criterion LSC [1], it still has been widely used as one measure to differentiate suspension type from each other (e.g., steel vs. air) [13, 14, 26]

De Pont points out that LSC does not address dynamic load-sharing [8]. The DLSC was proposed as an alternative to LSC to account for the dynamic nature of wheel-forces and instantaneous load-sharing during travel, and is defined as [8]

$$DLSC_i=\sqrt{\frac{\sum_{j=1}^{k}(DLS_i(j)-\frac{1}{k}\sum_{j=1}^{k}DLS_i(j))^2}{k}}, \tag{30}$$

The dynamic load-sharing of wheel i, $DLS_i(j)$, is

$$DLS_i(j)=\frac{nF_i(j)}{\sum_{i=1}^{n}F_i(j)}, \tag{31}$$

where n is the number of wheels on one side of an axle group; k is the number of terms in the dataset; and $F_i(j)$ is the instantaneous force at wheel i.

In this study, the average DLSC of tires on the same side of the semi-trailer axle group was employed as a metric of load-sharing. The average DLC of tires on the same side of the semi-trailer axle group was used to evaluate road-friendliness as well as to analyze the relationship between load-sharing and road-friendliness.

3.2 Model validation

The prototype of the tri-axle semi-trailer was tested on various road sections for verification of the integrated model of vehicle and road excitation, as shown in Figure 2. The tests were part of a joint project between Queensland University of Technology (QUT) and the Department of Transport and Main Roads, Queensland (TMR) [27].

The setups of the tests are shown in Figure 2 [27]. Two types of longitudinal connections were used to connect the passive air suspensions on the same side: conventional (three 6.5 mm inside diameter connectors connecting a 6.5 mm inside diameter air line) and large (three 20 mm inside diameter connectors connecting a 50 mm inside diameter air line). Strain gauges (one per hub) were mounted on the neutral axis of each axle between the spring and the hub to record the shear force on the hubs, i.e., air spring force, and accelerometers were mounted as closely as possible to each hub and to the corresponding upper positions at the chassis to derive the height of each air spring. In addition, six air pressure transducers were employed to obtain the pressures inside the air springs, and a TRAMANCO P/L on-board CHEK-WAY telemetry system was used to record all the data.

The dynamic force of each tire was derived based on the shear force on the respective hub and the acceleration on the respective axle. The effective area of each air spring was obtained by dividing the respective shear force by the respective pressure inside the air spring, and the volume of each air spring was derived by multiplying the respective effective area by the respective spring height.

The tests comprised driving the semi-trailer over three typical urban road sections at speeds ranging from 60 km/h to 80 km/h; the sections of road varied from smooth with long undulations to rough with short undulations. The IRI (international roughness index) values of each road section were provided by TMR, and the IRI is related to $G_q(n_0)$ in eq. (6) as $\mathrm{IRI} = 0.78\times10^3\sqrt{G_q(n_0)}$ [28]. Ten seconds of dynamic signal data were recorded per road section, and this

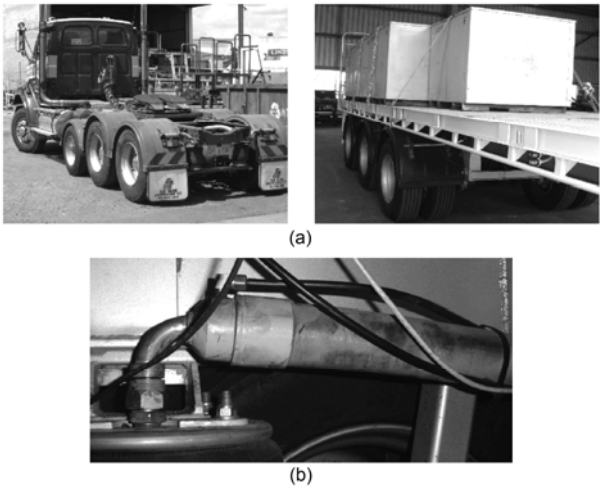

Figure 2 Setups of the tests. (a) Prime mover and test semi-trailer with test load; (b) large longitudinal air line.

was done for both experimental cases (i.e., conventional longitudinal connection vs. large longitudinal connection) for the fully loaded condition.

Thus, the dynamic effective area of each air spring is approximated as a function of the dynamic height of corresponding air spring y based on the experimental results, i.e.,

$$A_{s1} = -7.670500y^3 + 2.866880y^2 - 0.354226y + 0.093002. \quad (32)$$

The effective area multiplied by the dynamic spring height yields

$$V_{s1} = -7.670500y^4 + 2.866880y^3 - 0.354226y^2 + 0.093002y. \quad (33)$$

The comparisons between the test and simulation results in terms of load-sharing performance are listed in Table 2 and Figure 3.

As shown in Table 2 and Figure 3, a reasonable agreement exists between test and simulation results for both

Table 2 Tests and simulation results

Test/simulation number	Type of longitudinal connection	IRI	Velocity (km/h)	Load-sharing criteria	Test results	Simulation results	Error ratio (compared with the test results) (%)
1	conventional	6.213	60	DLC	0.0791	0.0733	−7.3
				DLSC	0.0505	0.0431	−14.6
2	large	6.213	60	DLC	0.0699	0.0637	−8.9
				DLSC	0.0440	0.0357	−18.8
3	conventional	7.602	70	DLC	0.1034	0.1001	−3.2
				DLSC	0.0851	0.0721	−15.3
4	large	7.602	70	DLC	0.0983	0.0926	−5.8
				DLSC	0.0819	0.0645	−21.2
5	conventional	8.880	80	DLC	0.1773	0.1679	−5.3
				DLSC	0.1506	0.1256	−16.6
6	large	8.880	80	DLC	0.1775	0.1626	−8.4
				DLSC	0.1474	0.1256	−14.8

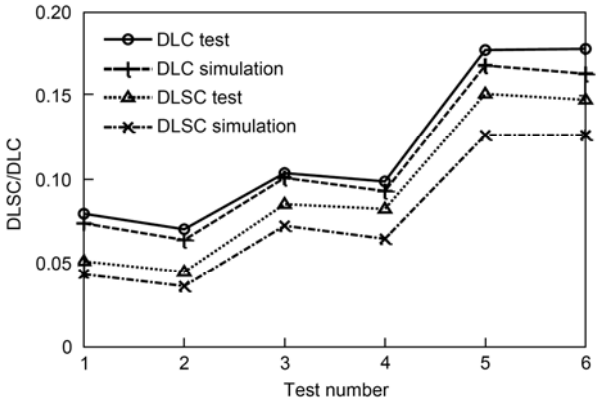

Figure 3 Comparison between test and simulation in terms of DLC and DLSC.

types of connection, under various road roughness conditions and vehicle speeds. The absolute error ratio of the DLC between each test and corresponding simulation is less than 10%; except for test/simulation 4, the absolute error ratios of the DLSC are less than 20%. It is also noted that all the simulation results are smaller than the corresponding test results, which is mainly due to wear of the suspensions of the test vehicle after a period of use and some simplifications of the model of longitudinal-connected air suspensions.

It can be concluded from Table 2 that the simulation results correlated well with the measurements. Therefore, the integrated model of vehicle and road excitation in this study can be employed for further analysis.

4 Effect of driving conditions on load-sharing

4.1 Effect of road roughness

The effects of road roughness on load-sharing were studied assuming the semi-trailer was fully-loaded with a constant vehicle speed of 20 m/s. Note that the diameters of air lines and connectors are between 4 mm and 10 mm for most semi-trailers in western countries [13]. Two types of connections among air suspensions were considered in this study, i.e., type "1" (three 6.5 mm inside diameter connectors connecting a 6.5 mm inside diameter air line) and type "2" (three 50 mm inside diameter connectors connecting a 50 mm inside diameter air line). The influence of road roughness (IRI varies from 2 to 9, representing road classes from "A" to "C") on the average DLSC and the average DLC are shown in Figure 4.

Figure 4(a) indicates that as the IRI increases, the average DLSC increases for suspensions with both types of connections. When the IRI increases from 2 to 11, the average DLSC of the semi-trailer with connection "1" increases from 0.0053 to 0.1558, and the average DLSC of the semi-trailer with connection "2" increases from 0.0049 to 0.1600. The reason for this phenomenon is that as the road roughness increases, the peak value of tire force increases, so it becomes more difficult for the air suspension to distribute the loads equally among all axles. As with the DLSC, the average DLC generally increases as IRI increases, as shown in Figure 4(b), except for a reduction when IRI is 9. It indicates that although there are correlations between the two criteria, the load-sharing performance criterion-

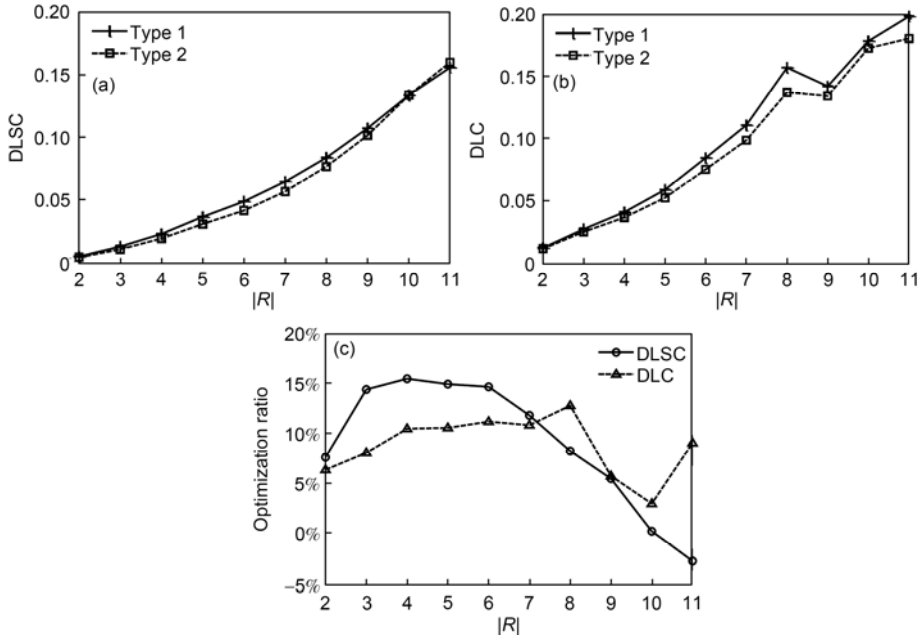

Figure 4 Effect of road roughness on load-sharing. (a) DLSC; (b) DLC; (c) DLSC optimization ratio and DLC.

DLSC is not always in accordance with the road-friendliness performance criterion-DLC.

The effect of road roughness on optimization ratios for load-sharing is shown in Figure 4(c). It is evident that the optimization ratio for DLSC does not necessarily increase or decrease as the IRI increases. When the IRI increases from 2 to 4, and then to 11, the optimization ratio for DLSC increases from 7.5% to 15.4%, and then declines to –2.7%. This phenomenon is further complicated by the fact that the main frequencies of the road profile excitations change with the roughness. When the IRI is low, most undulations are relatively long and accordingly low frequency road excitations are prominent, and are even lower than the transmission frequency of the air in connection "2", so a low DLSC optimization ratio is observed at first. As the IRI increases, the lower cut-off frequency of road excitation increases and more excitations reach the air transmission frequency, thus DLSC optimization ratio climbs until it reaches a peak value. As the dominant frequencies of road excitations continue to increase, air transmission becomes not fast enough to distribute loads equally among axles under the high frequency road excitations, the optimization ratio thus begins to decline, and even reaches a negative value.

The DLC optimization ratio in Figure 4(c) fluctuates more than the DLSC optimization ratio, with the most obvious difference being that the DLC optimization ratio increases again when the IRI reaches 11.

4.2 Effect of vehicle speed

Vehicle speeds varying from 20 km/h to 90 km/h were considered for simulations of the fully-loaded semi-trailer with a standard "A" class road profile.

The influence of vehicle speed on load-sharing is illustrated in Figure 5. As the speed increases from 20 km/h to 90 km/h, load-sharing of the semi-trailer with both types of air line deteriorates. The DLSC increases from 0.0040 to 0.0185 and 0.0028 to 0.0159 for the semi-trailer with connections "1" and "2", respectively, while the DLC increases from 0.0049 to 0.0373 and 0.0038 to 0.0337 for the semi-trailer with connections "1" and "2", respectively.

As shown in Figure 5(c), the DLSC optimization ratio fluctuates with vehicle speed. When vehicle speed increases from 20 km/h to 40 km/h, and then to 70 km/h, the DLSC optimization ratio decreases rapidly from 30.0% to 11.5% before it increases slowly to 15.2%. It then declines to 14.1% at 90 km/h. Similar changes in the DLC optimization ratio are found when speeds are less than 30 km/h, after that the DLC optimization ratio increases gradually.

A reasonable explanation for the variation patterns of DLSC and DLC optimization ratios is that the vehicle speed affects the product of the vehicle speed and the cutoff values of the roughness spatial frequency, i.e., un_1 and un_2, which means a higher vehicle speed results in higher upper and lower cut-off frequencies, as well as a wider frequency band. These changes have a complex influence on the transmission response of air inside the air line and the dynamic stiffness of each air spring.

4.3 Effect of vehicle load

The air springs of the semi-trailer are passive, which means the air springs do not deflate or inflate when the vehicle load changes. The load-sharing of the semi-trailer employ-

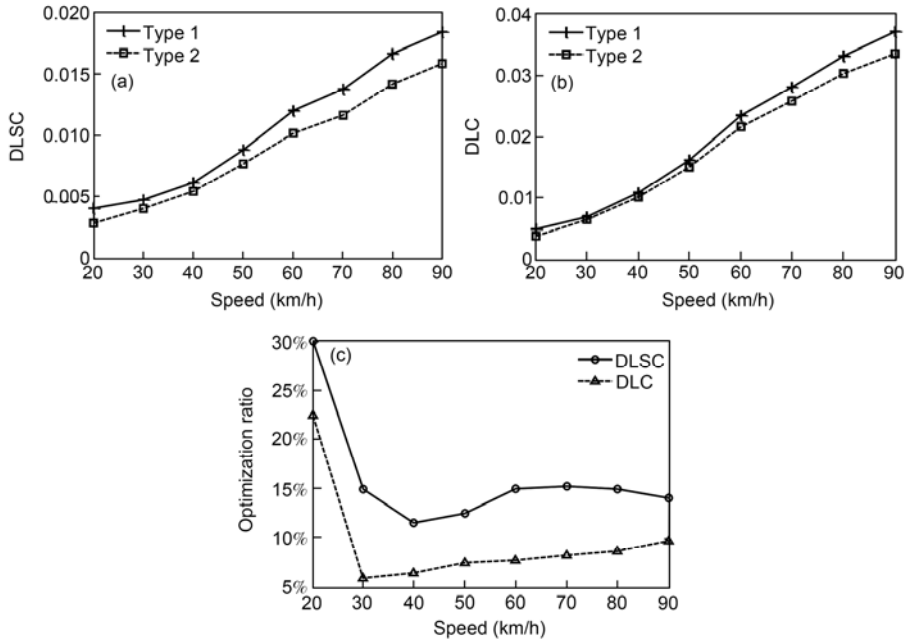

Figure 5 Effect of vehicle speed on load-sharing. (a) DLSC; (b) DLC; (c) DLSC optimization ratio and DLC.

ing two connections with five different loads is plotted in Figure 6. The vehicle is driving at 20 m/s on a standard "B" class road.

Figures 6(a) and (b) show that as the gross sprung mass decreases from 8700 kg to 5100 kg, increases of up to 40.3%, 62.2% are found in DLSC of the semi-trailer with "A", "B" connections respectively, and the DLC increases 21.4% and 33.4% for the semi-trailer with "A" and "B" connections, respectively. The variation pattern of DLC is consistent with previous studies [19, 29], and it is also concluded that as the vehicle load varies, the trend of DLSC follows the trend of DLC.

It is shown in Figure 6(c) that as the gross sprung mass decreases from 8700 kg to 5100 kg, the optimization ratio giving the relative advantage of connection "1" over connection "2" declines from 14.2% to 0.8%, and from 10.0% to 1.0%, for the DLSC and the DLC, respectively. In fact, as the vehicle load decreases, both h_{s10} and V_{s10} increase, and the volume of air line/V_{s10} decreases, such that the effect of employing the large air line and connectors becomes less prominent.

5 Effect of suspension parameters on load-sharing

5.1 Effect of static height and static pressure

The effect of the static height and static pressure of air springs for the fully-loaded semi-trailer are discussed in this section for a constant vehicle speed of 20 m/s and a standard "B" class road profile. The influence of the static height (varying from 0.15 m to 0.22 m) and corresponding static pressure (varying from 463431 Pa to 495204 Pa) on load-sharing are shown in Figure 7.

It can be seen in Figures 7(a) and (b) that both the DLSC and DLC reduce as the static height increases. In fact, when the static height increases, the absolute value of dA_{s10}/dy increases and dV_{s10}/dy decreases based on eqs. (32) and (33). These result in the reduction of dynamic stiffness of each air spring and accordingly the decline of DLSC and DLC.

Another finding is that compared with the DLC of the semi-trailer with connection "2", which decreases at a relatively constant rate, the DLSC of the semi-trailer with connection "2" decreases more slowly and becomes constant when the static height exceeds 0.19 m. This indicates that when a large connection is employed, the load-sharing will not change much as the static height increases and the air pressure of air springs decreases, but the dynamic tire forces will continue to reduce.

The optimization ratios of both DLSC and DLSC decline as the static height increases, as shown in Figure 7(c). The reason for this phenomenon is similar to the explanation for the phenomenon seen in Figure 6(c). As the static height increases, V_{s10} increases, and the volume of air line/V_{s10} decreases, and the effect of employing large air line and connectors becomes less prominent.

5.2 Effect of inside diameter of air line and connector

The effects of size of air line and connector (varying from 10 mm to 100 mm) on load-sharing are plotted in Figure 8, with a constant vehicle speed of 20 m/s for the fully-loaded semi-trailer and a standard "B" class road profile. The diameters of the connectors are always less than or equal to those of the air lines in all the simulations.

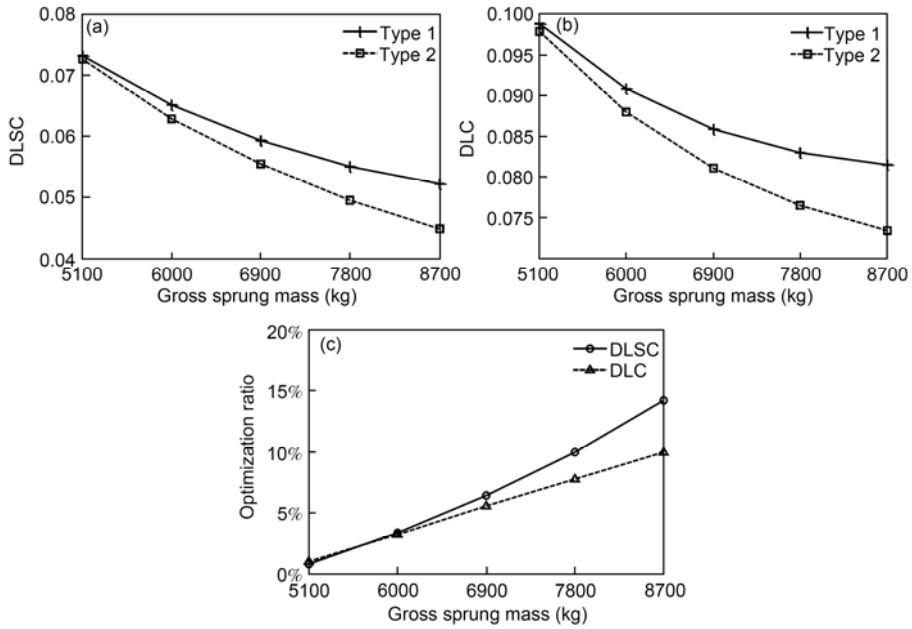

Figure 6 Effect of vehicle load. (a) DLSC; (b) DLC; (c) DLSC optimization ratio and DLC.

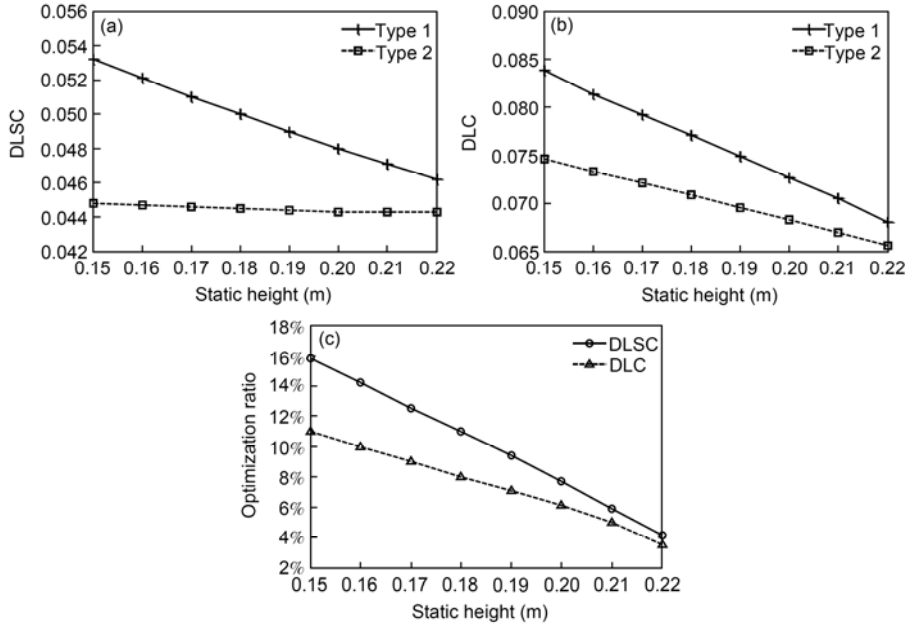

Figure 7 Effect of static height on load-sharing. (a) DLSC; (b) DLC; (c) DLSC optimization ratio and DLC.

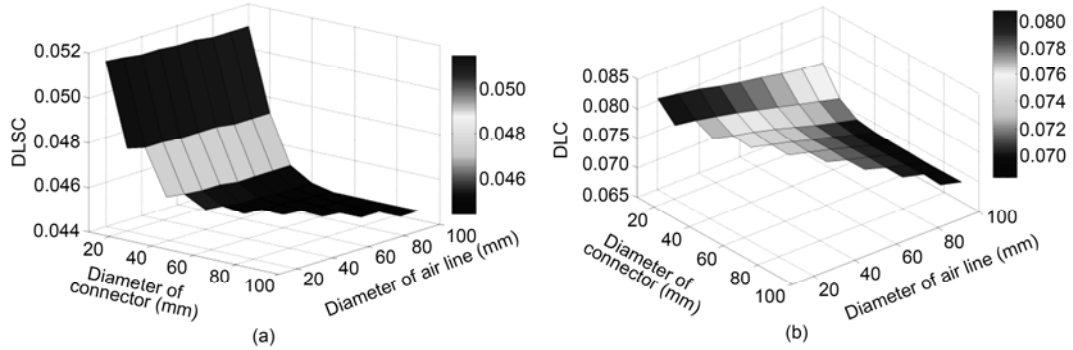

Figure 8 Effect of size of air line and connector on load-sharing optimization ratios. (a) DLSC; (b) DLC.

It can be seen in Figures 8(a) and (b) that with a fixed diameter of air line, both DLSC and DLC reduce quickly as the air line diameter increases from 10 mm to 30 mm. For example, with a 100 mm diameter air line, reductions up to 11.4% and 8.4% are observed for DLSC and DLC, respectively. When the diameter of air line increases beyond 30 mm, both DLSC and DLC decrease more slowly and finally become constant.

However, when the diameter of the connector is fixed, the change of DLSC with air line diameter is different from that of the DLC. With a 10 mm diameter connector, as the air line diameter increases from 10 mm to 100 mm, the DLSC only decreases 1.0%, while the DLC decreases 6.8%. Thus, although the load-sharing of the semi-trailer improves very slowly by increasing the size of the connector, the dynamic tire force and accordingly the road-friendliness of the semi-trailer are effectively improved.

6 Conclusions

In this study, the effects of suspension parameters and driving conditions on dynamic load-sharing of longitudinal-connected air suspensions of a tri-axle semi-trailer were investigated comprehensively. A novel nonlinear model of longitudinal-connected tri-axle air suspensions was formulated based on fluid mechanics and thermodynamics and validated through test results. The effects of road surface conditions, driving speeds, air line diameters and connector diameters on the dynamic load-sharing capability of the semi-trailer were analyzed in terms of the DLSC and DLC, and the following conclusions can be drawn:

1. Although the two criteria are correlated in most cases, the road-friendliness metric–DLC is not always in accordance with the load-sharing metric–DLSC.

2. The DLSC optimization ratio by employing larger air lines and connectors varies as the road roughness or vehicle

speed changes. The lower and upper cut-off frequencies of road excitation change with the IRI and vehicle speed, which has a complicated impact on air transmission between air bags and thus the damping of the each air bag.

3. When the vehicle load is reduced, or the static pressure is increased, the DLSC optimization ratio declines. The reason for this phenomenon is that the static height increases with lighter vehicle load or less static pressure, V_{s10} increases, and the volume of air line/V_{s10} decreases. Thus, the effect of employing a large air line and connectors becomes less prominent.

4. If the diameter of the air line is always larger than that of the connector, then the influence of the diameter of air line is more significant than that of the connector.

Based on the proposed model, investigation into the mechanism of load-sharing based on the nonlinear system dynamics and the control methods of the tri-axle air suspension system with longitudinal air line will be undertaken in the future.

This work was supported by the National Natural Science Foundation of China (Grant Nos. 51078087, 51178158, and 51075112), the Natural Science Foundation of Anhui Province (Grant No. 11040606Q39), and the Fundamental Research Funds for the Central Universities (Grant Nos. 2012HGQC0015 and 2011HGBZ0945). The assistance of Dr Lloyd Davis from the Queensland Department of Transport and Main Roads is also greatly acknowledged.

1 Davis L E, Bunker M B. Load-sharing in heavy vehicle suspensions–New metrics for old. Queensland University of Technology, QUT Digital Repository, Brisbane, Australia, 2008
2 Potter T E C, Cebon D, Cole D J, et al. Road damage due to dynamic tyre forces, measured on a public road. Int J Heavy Veh Syst, 1996, 3: 346–362
3 Cebon D. Assessment of the dynamic wheel forces generated by heavy road vehicles. Symposium on Heavy Vehicle Suspension Characteristics, Canberra, Australia, 1987. 199–212
4 Cantieni R, Krebs W, Heywood R. Dynamic interaction between vehicles and infrastructure experiment (divine), Technical Report No. DSTI/DOT/RTR/IR6(98)1/FINAL. Organisation for Economic Co-operation and Development (OECD), Paris, France, 1998
5 Department of Transport and Regional Services, Australia. Vehicle Standards Bulletin VSB 11 Certification of road-friendly suspension systems. Australian Department of Infrastructure, Transport, Regional Development and Local Government, Canberra, Australia, 2004
6 Costanzi M, Cebon D. An investigation of the effects of lorry suspension performance on road maintenance costs. P I Mech Eng C-J Mec, 2007, 221: 1265–1277
7 Sweatman P F. A study of dynamic wheel forces in axle group suspensions of heavy vehicles. Australian Road Research Board, Special report. Report No. SR27. Vermont South, Victoria, Australia
8 de Pont J. J. Assessing heavy vehicle suspensions for road wear. Research report No. 95. Transfund New Zealand, Wellington, New Zealand, 1997
9 Potter T E C, Cebon D, Collop A C, et al. Road-damaging potential of measured dynamic tyre forces in mixed traffic. P I Mech Eng D-J Aut, 1996, 210: 215–225
10 OECD Scientific Expert Group. Dynamic loading of pavements: Road transport research. Organization for Economic, Paris, France, 1992
11 Estill & Associates Pty Ltd. Operational stability and performance of air suspension on various vehicle configurations. Australia: Department of Transport and Works, South Perth, WA, Australia, 2000
12 Roaduser Systems Pty Ltd. Stability and on-road performance of multi-combination vehicles with air suspension systems. Australia: National Road Transport Commission, Canberra, Australia, 2005
13 Davis L E. Heavy vehicle suspensions-testing and analysis. Dissertation for the Doctoral Degree. Brisbane: Queensland University of Technology, 2010
14 Davis L E, Bunker J M. Altering heavy vehicle air suspension dynamic forces by modifying air lines. Int J Heavy Veh Syst, 2011, 18: 1–17
15 Roebuck R L, Cebon D, Dale S G. Optimal control of a semi-active tri-axle lorry suspension. Veh Syst D, 2006, 44: 892–903
16 Zhao W Z, Wang C Y. Mixed H_2/H_∞ road feel control of EPS based on genetic algorithm. Sci China Tech Sci, 2012, 55: 72–80
17 Lu Y J, Yang S P, Li S H. Research on dynamics of a class of heavy vehicle-tire-road coupling system. Sci China Tech Sci, 2011, 54: 2054–2063
18 Romero J A, Lozano A. Effect of truck suspension and tire properties on pavement damage spatial distribution." Transport Res Rec, No. 1949, Transportation Research Board of the National Academies, Washington, D.C., 2006, 148–154
19 Shi X M, Cai C S. Simulation of dynamic effects of vehicles on pavement using a 3d interaction model. J Transp Eng-ASCE, 2009, 135: 736–744
20 ISO. Mechanical vibration—road surface profiles-reporting of measured data. ISO 8068: 1995 (E), Geneva, 1995
21 Chen J P, Chen W W, Zhu H, et al. Modeling and simulation on stochastic road surface irregularity based on Matlab/Simulink. Trans Chin S Agr Mach, 2010, 41: 11–15
22 Prabakar R S, Sujatha C, Narayanan S. Optimal semi-active preview control response of a half car vehicle model with magnetorheological damper. J Sound Vib, 2009, 326: 400–420
23 Wang J S, Zhu S H. Linearized model for dynamic stiffness of air spring with auxiliary chamber. J Vib Shock, 2009, 28: 72–76
24 White F M. Fluid Mechanics. Columbus: McGraw-Hill, 2011
25 Chen S M. Hydraulic and Pneumatic Transmission. Beijing: China Machine Press, 2011
26 Davis L E, Bunker J M. Suspension Testing of 3 Heavy Vehicles-Dynamic Wheel Force Analysis–Report. Australia: Department of Main Roads-Queensland Government, Brisbane, Australia, 2009
27 Davis L E, Bunker J M. Heavy vehicle suspension testing and analysis-dynamic load sharing. Australia: Department of Main Roads-Queensland Government, Brisbane, Australia, 2009
28 Chen H X, He Z Y. A study on simulation of road roughness based on international roughness index. Highway, 2008, 11: 155–160
29 Lu Y J, Yang S P, Li S H, et al. Numerical and experimental investigation on stochastic dynamic load of a heavy duty vehicle. Appl Math M, 2010, 34: 2698–2710